



## ORIGINAL ARTICLE

# Cancer-derived exosomal circTMEM56 enhances the efficacy of HCC radiotherapy through the miR-136-5p/STING axis

Li Yuan<sup>1\*</sup>, Yue Wang<sup>1\*</sup>, Junjie Cheng<sup>2\*</sup>, Shilin Lin<sup>1</sup>, Aying Ma<sup>1</sup>, Kunchao Li<sup>3</sup>, Yiming Zheng<sup>1</sup>, Zhaochong Zeng<sup>4</sup>, Aiwu Ke<sup>1</sup>, Chao Gao<sup>1</sup>, Shisuo Du<sup>4</sup>

<sup>1</sup>Liver Cancer Institute, Zhongshan Hospital, Fudan University, Key Laboratory of Carcinogenesis and Cancer Invasion (Fudan University), Ministry of Education, Shanghai 200032, China; <sup>2</sup>Graduate School of Bengbu Medical University, Bengbu 233030, China; <sup>3</sup>Department of Cardiovascular Surgery, The Second Affiliated Hospital of Nanchang University, Nanchang 330000, China; <sup>4</sup>Department of Radiation Oncology, Zhongshan Hospital, Fudan University, Shanghai 200032, China

### ABSTRACT

**Objective:** Although the role of circular RNAs (circRNAs) in tumor progression and immune regulation is well-known, the specific circRNA molecules that mediate immune responses after radiotherapy (RT) and the underlying mechanisms have not been identified.

**Methods:** Cytometry with time-of-flight (CyTOF) was used to analyze blood samples from patients with liver cancer exhibiting abscopal effects (AEs) after stereotactic body radiotherapy (SBRT) to quantify the number of dendritic cells (DCs) and CD8<sup>+</sup> T cells and interferon-beta (IFN- $\beta$ ) level. circTMEM56 and IFN- $\beta$  levels were measured in 76 patients with liver cancer using qPCR and ELISA. Immunohistochemistry validated circTMEM56 and CD141 staining in tissues. The interaction between circTMEM56, miR-136-5p, and STING, as well as the impact on anti-tumor immunity, was verified using circTMEM56-specific probes, dual-luciferase activity assays, proteomics analysis, and western blot analysis.

**Results:** The role of circTMEM56 in enhancing anti-tumor immunity and response to RT in hepatocellular carcinoma (HCC) was determined. Higher circTMEM56 levels were linked to an improved RT response and better clinical outcomes in patients with HCC. circTMEM56 enhanced cGAS-STING signaling, increased the number of tumor-infiltrating CD8<sup>+</sup> T cells, and elevated the serum IFN- $\beta$  levels. Moreover, circTMEM56 administration significantly boosted the response to RT in tumors with low circTMEM56 expression.

**Conclusions:** High circTMEM56 expression in HCC modulates the distant effects of HCC RT by activating the cGAS-STING pathway to reshape the tumor microenvironment. This study provides a new approach to improve RT efficacy for HCC.

### KEYWORDS

circTMEM56; hepatocellular carcinoma; cGAS-STING; radiotherapy; dendritic cell

## Introduction

Liver cancer has the third highest cancer-related mortality rate according to the 2022 global cancer statistics<sup>1</sup>. The most common type of liver cancer is hepatocellular carcinoma (HCC), which is usually diagnosed at an advanced stage and

is challenging to treat<sup>2</sup>. Moreover, postoperative recurrence rates following radical surgical resection remain high, making locoregional and systemic therapies key components in HCC management. Radiotherapy (RT) is a reliable and effective treatment for HCC, providing excellent local control and converting unresectable tumors into resectable tumors, thus improving therapeutic outcomes. Recent advances in novel RT technology, including image-guided radiotherapy (IGRT), intensity-modulated radiotherapy (IMRT), and stereotactic body radiotherapy (SBRT), have significantly expanded the scope of RT. Traditionally viewed solely as a cytotoxic treatment, RT has evolved to profoundly influence the tumor immunoenvironment. For example, the abscopal effect (AE) demonstrates the potential of immunomodulators to enhance the therapeutic value of RT, giving rise to a new field of study known as immunoradiotherapy<sup>3</sup>. Despite the significant

\*These authors contributed equally to this work.

Correspondence to: Aiwu Ke, Chao Gao and Shisuo Du

E-mail: keaiwu\_fd@hotmail.com, gachao\_4068@163.com and du.shisuo@zs-hospital.sh.cn

ORCID ID: <https://orcid.org/0000-0002-7964-6909>, <https://orcid.org/0000-0002-8381-7416> and <https://orcid.org/0009-0007-5295-3064>

Received November 22, 2024; accepted February 26, 2025;

published online April 23, 2025.

Available at [www.cancerbiomed.org](http://www.cancerbiomed.org)

©2025 The Authors. Creative Commons Attribution-NonCommercial 4.0 International License

improvement in abscopal response rates achieved by combining RT with immunotherapeutic agents, the underlying mechanisms have not been established.

Circular RNAs (circRNAs) are thought to be products of splicing in mammalian cells, where thousands of circRNAs are associated with diverse biological functions, including microRNA (miRNA) sponging<sup>4</sup>. As a result, circRNAs are dysregulated in several diseases, including cancer<sup>5</sup>. Several genes, such as circTRIM33-12 and circMET, have been implicated in HCC progression<sup>6</sup>. circRNAs are known to be stable and enriched in exosomes. Evidence suggests that exosome circRNA dysregulation affects exosome-mediated intracellular communication, especially during tumor development. For example, HCC cells are immunosuppressed by exosome circUHRH1, whereas non-small cell lung cancer (NSCLC) cells are dysregulated by exosome circUSP7 and resist anti-PD-1 therapy<sup>7</sup>. Although circRNAs have an important role in the therapeutic efficacy of RT, the impact of circRNAs on RT effectiveness is not known. Further research is needed to clarify how circRNAs influence the therapeutic outcomes of RT in HCC.

Cells in malignant tumors survive immune attacks through mechanisms, such as loss of immunogenicity and immunosuppression<sup>8</sup>. Immune evasion is a hallmark of cancer cells. The interplay between tumor cells and the immune system has a crucial role during advanced cancer stages<sup>9</sup>. Additionally, immune checkpoint blockade (ICB) therapies have been shown to improve the prognosis of cancer by effectively targeting and eliminating cancer cells<sup>10</sup>. Anti-PD-1 antibody, for example, is approved as second-line therapy for advanced HCC<sup>11</sup>. However, anti-PD-1 treatment achieves complete or partial responses in only 17%–18% of patients with advanced HCC and the numerous adverse events underscore the need for a deeper understanding of HCC-related immunosuppression<sup>12</sup>.

Pre-RT specimens and blood samples from six patients with metastatic HCC were analyzed. Three patients reported AEs, while three had tumor progression. These cases were selected for circRNA sequencing to identify differentially expressed circRNAs to better understand how RT affects the tumor immunoenvironment by identifying critical circRNAs. Ultimately, the current study aimed to assess the efficacy of RT and propose a novel combined treatment strategy for improving RT outcomes in patients with HCC.

## Materials and methods

### Samples

From January 2016 to December 2020 fresh puncture specimens were collected from patients with HCC before surgery or RT. Blood samples were collected using EDTA tubes and all specimens were promptly stored at  $-80^{\circ}\text{C}$ . Our previous study outlined the creation of tumor microarrays and subsequent follow-up protocols<sup>13</sup>. Ethical approval was obtained from the Institutional Review Board of Zhongshan Hospital [Fudan University, Shanghai, China (Approval no. ZS20240204)].

### Cell lines and transfection

Human HCC cell lines (HepG2, Hep3B, Huh7, PLC/PRF/5, HCCLM3, and MHCC97H) and mouse HCC cell lines (Hepa 1–6) were sourced from the Chinese Academy of Science Cell Bank (Shanghai, China). Cell lines were cultured in DMEM or RPMI-1640 medium supplemented with 10% fetal bovine serum and 1% antibiotics at  $37^{\circ}\text{C}$  in a humidified incubator with 5%  $\text{CO}_2$ .

Shanghai Genomeditech Company (Shanghai, China) provided the vectors. HCCLM3 cells were transfected with circTMEM56 shRNA lentiviral and control vectors. circTMEM56 cDNA vectors and the corresponding control vectors were transfected into Hep3B and Hep1-6 cell lines, which were also constructed by Shanghai Genomeditech Company. The circTMEM56 shRNA target sequences were 5'-GTGAATCAGCGGTTGAAGAAA-3' (shRNA1), 5'-GTTTGTGAATCAGCGGTTGAA-3' (shRNA2), and 5'-GAATCAGCGGTTGAAGAAATA-3' (shRNA3). The STING shRNA target sequences were 5'-CAGCATTACAACAACCTGCTA-3' (shRNA1), 5'-CTGCTCGTAGCGCCGGGCCTT-3' (shRNA2), and 5'-GACCGGTGACCATGCTGGCAT-3' (shRNA3). Antibiotic-resistant transfected cells were selected by adding puromycin to the culture medium for 7 d.

### RNA-seq and analysis

A Ribo-Zero kit (Illumina, San Diego, CA, USA) was used to deplete total RNA of rRNA. An Illumina TruSeq RNA Sample Prep kit (Illumina, San Diego, CA, USA) was used to prepare cDNA libraries from total RNA. Sequencing was performed

using an Illumina HiSeq2500 platform by GeneWiz (Suzhou, Jiangsu, China). CIRI software (version 2; BGI, Shenzhen, Guangdong, China) was used to identify circRNAs with the sequencing reads aligned to the GRCh38 reference genome. Count data and differentially expressed circRNAs (DE circRNAs) were analyzed in a previous study<sup>13</sup>.

### ***In situ* hybridization**

Slides were deparaffinized, rehydrated, digested with pepsin, and subsequently dehydrated before hybridization with 50-nm locked nucleic acid (LNA)-modified DIG-labeled probes specific to circTMEM56. The slides were washed three times after hybridization, soaked in blocking buffer, and incubated with alkaline phosphatase-conjugated anti-DIG Fab fragments. The nuclei were stained with nuclear fast red.

### **SILAC**

Cells were cultured and labeled using SILAC kits (Invitrogen, Carlsbad, CA, USA). After harvesting an equal number of cells from both groups were combined for crude protein extraction. The peptides were analyzed using nano-HPLC-MS/MS using a Q Exactive mass spectrometer (Thermo Fisher Scientific, city, state, country). Acquired MS/MS data were processed with MaxQuant software (Shanghai Institute of Biochemistry and Cell Biology, Shanghai, China) using the Andromeda search engine (v.1.3.0.5). The reverse decoy database and protein sequences of common contaminants were concatenated using the UniProtKB mouse database (43,233 sequences).

### **Mice tumor challenge and RT treatment**

HCC cells were used to create subcutaneous or *in situ* xenograft mouse models. A radiation dose (10 Gy) was administered to assess the response to RT<sup>14</sup>. Subcutaneous xenograft growth was monitored every 3 d, while *in situ* xenograft volume was measured on day 25 after injection. Six mice per group were sacrificed on day 25 after inoculation.

### **Real-time quantitative PCR (qRT-PCR), immunohistochemistry (IHC), and immunoblot (IB) analyses**

SYBR Green Real-time PCR Master Mix (Yeasen, Shanghai, China) was used to extract RNA from tissues or cell lines.

The PCR primers were specific for circTMEM56 (forward: 5'-TGCTGGCATACATTGGGAAT-3', reverse: 5'-GCTGAAAGGTGAAAAAGCTGA-3'), GADPH (forward: 5'-GGTATGACAACGAATTTGGC-3', reverse: 5'-GAGCACAGGGTACTTTATTG-3'), TMEM173 (forward: 5'-TTTGCCATGT CACAGGATGC-3', reverse: 5'-ATGAGGCGGCAGTTATT TCG-3'), and cGAS (forward: 5'-TGGTGGGAAGAGTGGT GATTTC-3', reverse: 5'-TGCATTCCAATGGCAGAAGC-3'). IHC analysis was conducted following established protocols, as outlined in our previous study, using qualitative criteria for staining intensity. The integrated optical density (IOD) values were quantified using Image Pro Plus software (Media Cybernetics, Rockville, MD, USA) based on our previous research findings. IB analysis was performed<sup>15</sup> and relative protein expression was determined using ImageJ software.

### **Cell migration, matrigel invasion, and cell proliferation assays**

Cell migration and Matrigel invasion assays were performed as reported in earlier studies. For the cell proliferation assay,  $2 \times 10^3$  cells were seeded into 96-well plates and monitored at designated time intervals. Cell Counting Kit-8 [CKK-8] (Yeasen, Shanghai, China) was used to determine the optical density (OD).

### **Immunofluorescent staining and flow cytometry assays**

Immunofluorescence staining was performed on HCC cells as previously described. flow Cytometric analysis was used to determine apoptosis rates. The cells were stained with Annexin V-FITC/PI. Cells located in the lower-right quadrant were classified as Annexin V-positive and identified as early apoptotic cells, whereas cells in the upper-right quadrant, which were positive for both Annexin V and PI, were identified as late apoptotic cells. The resistance of these cells to apoptosis was assessed in both quadrants.

### **Tumor growth *in vivo***

Four-week-old nude mice were obtained from the Shanghai Institute of Material Medicine (Shanghai, China) and housed in a pathogen-free animal facility. A total of  $5 \times 10^6$  HCC cells were injected into nude mice to induce tumor growth. Tumor growth was monitored every 5 d post-injection until day 32 by measuring tumors bi-dimensionally, as described in our previous study.

Lung tissue sections were stained with hematoxylin and eosin (H&E) and the metastasis rate was determined using established methods. All the mouse experiments performed at Zhongshan Hospital were approved by the Fudan University Animal Ethics Committee (Approval no. ZS-Y2022-323).

## Dual luciferase reporter assay

Mutant luciferase reporter vectors were constructed using a mutagenesis kit (Qiagen, Hilden, Germany) according to the manufacturer's instructions. The plasmid was transiently transfected into 293T cells, which were lysed and collected after 48 h. The samples were centrifuged at  $8,944\text{--}20,124 \times g$  for 3–5 min to obtain the supernatants.

Luciferase was detected according to the instrument guidelines with a measurement duration of 10 s and an interval of 2 s. The assay involved gently mixing the sample with Firefly Luciferase Assay reagent (Beyotime Biotechnology, Shanghai, China) two-to-three times, followed by measuring relative light units (RLUs) using cell lysis buffer as a blank control. This procedure was repeated using Renilla Luciferase Assay reagent (Beyotime Biotechnology, Shanghai, China) and the RLU values were calculated as a measure of reporter gene activation.

## Statistical analysis

Quantitative data analysis was performed using SPSS 21.0 (SPSS, Inc., city, state, country). The two groups were compared using a Student's t-test. The Pearson correlation coefficient was used to assess the association between the two proteins, while the Kaplan-Meier method and log-rank test were used to analyze the overall survival and cumulative recurrence rates. Statistical significance was set at a  $P < 0.05$ . Student's t-test was used to determine statistical significance unless otherwise specified. Quantification data are presented as the mean value  $\pm$  SEM or in box-and-whisker plots with box dimensions encompassing the 25<sup>th</sup>–75<sup>th</sup> percentiles. Horizontal bars represent the median and error bars represent the minimum and maximum values.

## Results

### circTMEM56 downregulation is associated with a poor RT response and prognosis in patients with HCC

AEs describe the phenomenon in which RT at one location causes tumor regression in non-irradiated areas. According

to Response Evaluation Criteria in Solid Tumors 1.1, three patients who developed AEs after SBRT were enrolled between January 2016 and December 2020. Blood samples from these patients were analyzed by cytometry using time-of-flight (CyTOF), which revealed a higher number of dendritic cells (DCs) and CD8<sup>+</sup> T cells (**Figure 1A**). Patients with AEs had a higher interferon-beta (IFN- $\beta$ ) level and number of DCs, indicating that RT-induced AEs are related to systemic anti-tumor immunity (**Figure 1B–D**). The circRNA profiles from tumors and blood samples of patients with and without AEs following SBRT (**Figure 1E**) identified 89 DE circRNAs ( $\log_2|\text{FC}| > 1$ ,  $q\text{-value} < 0.05$ ; **Figure 1E**, right panel). By overlapping the two circRNA profiles, circRNA hsa\_circ\_0005720 (circTMEM56), derived from TMEM56, was shown to be the most upregulated circRNA in both tumor tissues and blood samples from patients with AEs (**Figure 1F**). qPCR and Sanger sequencing were performed to identify the loop structure of circTMEM56 using specific primers (**Figure 1G, H**). The circTMEM56 level in HCC tissues and blood samples from these patients was determined and shown to be higher in patients with AEs compared to patients without AEs (**Figure 1I–K**). circTMEM56 expression was further investigated using puncture samples from 30 patients with HCC receiving SBRT, which was shown to be low in most cases (**Figure 1L**).

In addition, circTMEM56 expression in HCC samples was determined. Semi-quantitative *in situ* hybridization microarray analysis showed significantly reduced circTMEM56 expression in HCC tissues (**Figure 1M**). Kaplan-Meier analysis showed that HCC patients with lower circTMEM56 expression (above the median) had significantly shorter survival ( $P = 0.0052$ ) and higher recurrence rates after RT compared to patients with higher circTMEM56 expression (**Figure 1N**). Based on these data, low circTMEM56 expression contributed to HCC progression by modulating RT response.

### Serum exosome circTMEM56 level correlates with the RT effect in patients with HCC

Circular RNAs have recently been shown to be highly concentrated in exosomes, exhibiting remarkable stability and abundance. Exosomes are naturally found in various cells, where exosomes mediate cell-to-cell communication and participate in multiple tumor development processes. We previously showed that circTMEM56 is upregulated in patients with AEs compared to patients without AEs. Herein the exosome levels of circTMEM56 in these patients was further examined (**Figure 2A, B**) and confirmed to be elevated in patients with



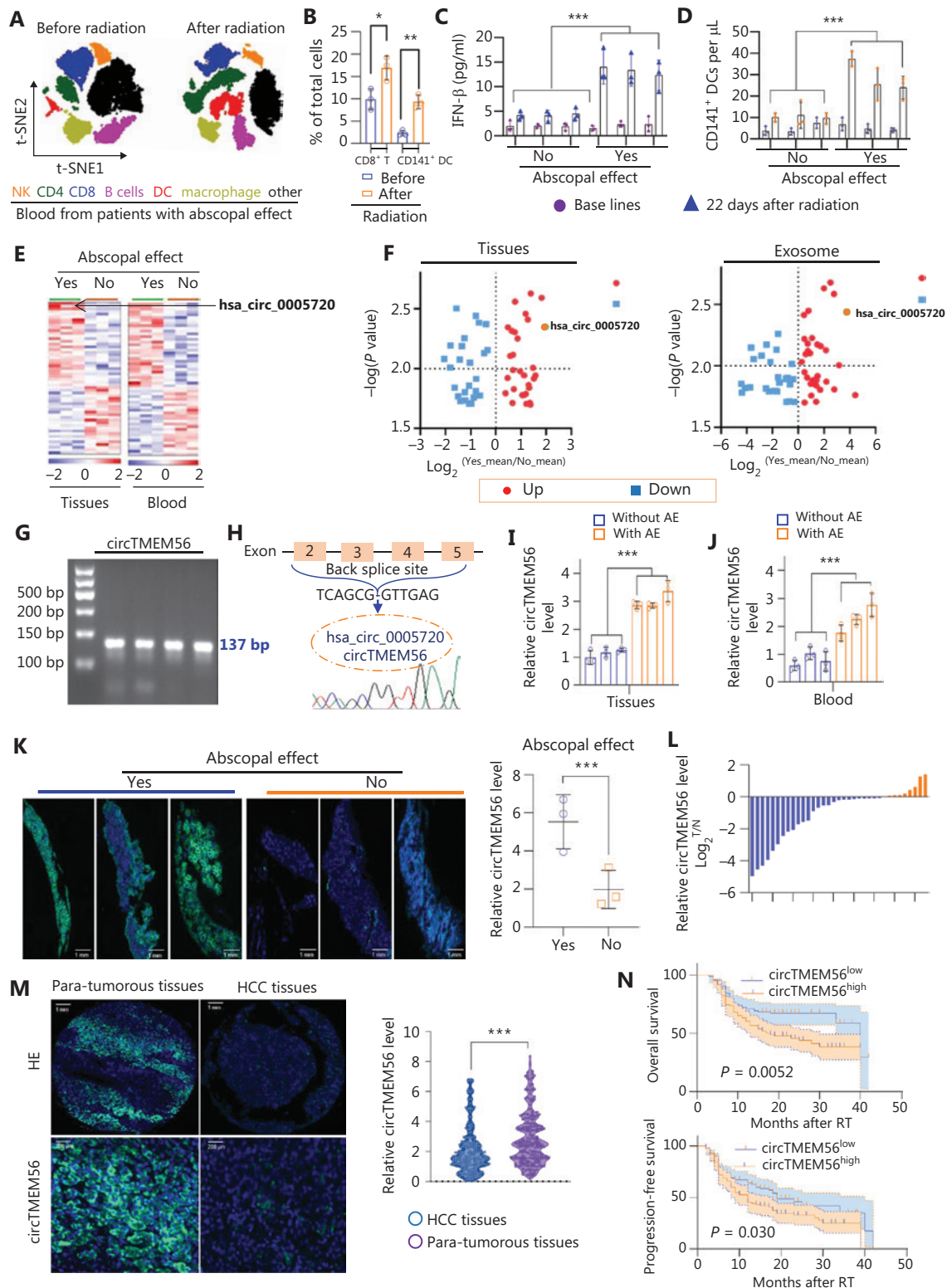


**Figure 1** Downregulation of circTMEM56 is associated with a poor radiotherapy (RT) response and prognosis in patients with liver cancer. (A) t-SNE diagram of CD45<sup>+</sup> major tumor-infiltrating immune cell types in patients with and without abscopal effects (AEs). (B) CD8<sup>+</sup> T cell level and number of dendritic cells (DCs) in the blood of patients with and without AEs. (C) IFN- $\beta$  level in the blood of patients with and without AEs. (D) Peripheral blood CD141<sup>+</sup> DCs (cDC1 subset) levels in AE-positive versus AE-negative patient cohorts. (E) Heat maps of circRNA expression in tumor tissues of liver cancer patients with and without AEs after RT. (F) Differentially expressed circRNAs identified in tumor

tissues and plasma exosomes of patients with and without AEs. (G) qPCR results showing circTMEM56 transcribed using primers from cDNA. (H) Schematic diagram of circTMEM56. Sanger sequencing revealed back-splicing sites. (I) qPCR results showing significantly higher circTMEM56 expression in hepatocellular carcinoma (HCC) tissues of patients with AEs compared to patients without AEs. (J) qPCR results showing significantly higher circTMEM56 expression in the blood of patients with AEs compared to patients without AEs. (K) *In situ* hybridization results indicating significantly higher expression of circTMEM56 in HCC tissues of patients with AEs compared to patients without AEs. (L) Variations in circTMEM56 expression in 30 HCC tissues and adjacent tissues. (M) *In situ* hybridization results showing significantly lower circTMEM56 expression in HCC tissues compared to para-cancer tissues. (N) Kaplan-Meier analysis of overall survival (OS) and progression-free survival (PFS) in 209 HCC patients was performed based on circTMEM56 expression. \* $P < 0.05$ ; \*\* $P < 0.01$ ; \*\*\* $P < 0.001$ .

AEs (**Figure 2B**). In addition, the exosome levels of circTMEM56 in blood after RT was determined in 76 patients with HCC. The circTMEM56 level was shown to be high in patients with a partial response (PR) and complete response (CR), moderate in patients with stable disease (SD), and low in patients with progressive disease (PD) (**Figure 2C**). Furthermore, blood samples from patients with a PR and CR had a higher IFN- $\beta$  level and greater number of DCs compared to patients with PD (**Figure 2D, E**). The exosome circTMEM56 level was positively associated with the IFN- $\beta$  level and number of conventional type 1 dendritic cells (cDC1s) (**Figure 2F, G**). Tumor tissues from patients with a PR and CR showed higher DC infiltration following SBRT than tissues from patients with PD and SD with a corresponding increase in the IFN- $\beta$  level and number of CD141<sup>+</sup> cells in the blood (**Figure 2H**). Additionally, the relationship between the blood exosome circTMEM56 level and response to RT was determined in 60 patients. A positive correlation existed between the blood exosome circTMEM56 and IFN- $\beta$  levels in patients with RT (**Figure 2I**), suggesting that the exosome circTMEM56 level is positively correlated with the response to RT in patients with HCC.

### Elevated circTMEM56 amplifies the RT-induced anti-tumor immune response *via* regulated type I IFN (IFN-I) production in DCs

Elevated circTMEM56 levels may improve the radiation response and efficacy by regulating IFN-I induction in DCs. The first step was to determine the endogenous circTMEM56 levels in seven HCC cell lines. Most HCC cell lines, especially HCC cell lines with high metastatic potential, exhibited lower circTMEM56 levels compared to the HepG2 cell line. Next, stable HepG2 and HCCLM3 cells were generated with circTMEM56 knockout or overexpression (**Figure 3A, B**). In addition to clinical efficacy, RT induces DNA damage, releasing

double-stranded DNA (dsDNA), which leads to tumor cell death and enhances local and distant tumor control *via* cancer cell-extrinsic mechanisms, such as the augmentation of tumor-specific immunity. Graded RT doses (0, 2, 4, 8, and 10 Gy) increased the dsDNA concentration in the supernatant of HCCLM3 cells in a dose-dependent manner (**Figure 3C, D**). Additionally, IFN- $\beta$  and dsDNA release in HCCLM3 cells following RT were not influenced by circTMEM56 expression (**Figure 3E, F**).

HCC cells were co-cultured with different circTMEM56 and DCs isolated from healthy human blood using microbeads to determine how circTMEM56 activates DCs and produces IFN- $\beta$ . IFN- $\beta$  and cDC1 cells were increased as a result of circTMEM56 overexpression, an effect that was inhibited by GW4869. This finding suggests that RT-induced anti-tumor immune responses and IFN-I production are enhanced in HCC cells expressing circTMEM56 (**Figure 3G–J**).

### circTMEM56 enhances RT-induced anti-tumor immune responses in HCC through the miR-136-5p/STING1 axis

Given that circRNAs function as miRNA sponges, whether circTMEM56 sponges target specific miRNAs to modulate HCC progression was investigated<sup>16</sup>. circTMEM56-interacting miRNAs were isolated using DCs and circTMEM56-specific probes and qRT-PCR was used to detect 385 potential miRNAs (Starbase v3.0). circTMEM56 specifically enriched miR-136-5p compared to the negative control (**Figure 4A**). A dual-luciferase reporter assay was performed in HEK293T cells to verify that miR-136-5p is sponged by circTMEM56. Wild type (WT) and mutant circTMEM56, lacking miR-136-5p binding sites, were cloned in the luciferase reporter vector, pLG3 (**Figure 4B**). The miR-136-5p mimic significantly reduced luciferase activity in WT-circTMEM56 but not in mutant-circTMEM56 (**Figure 4C**). Additionally,

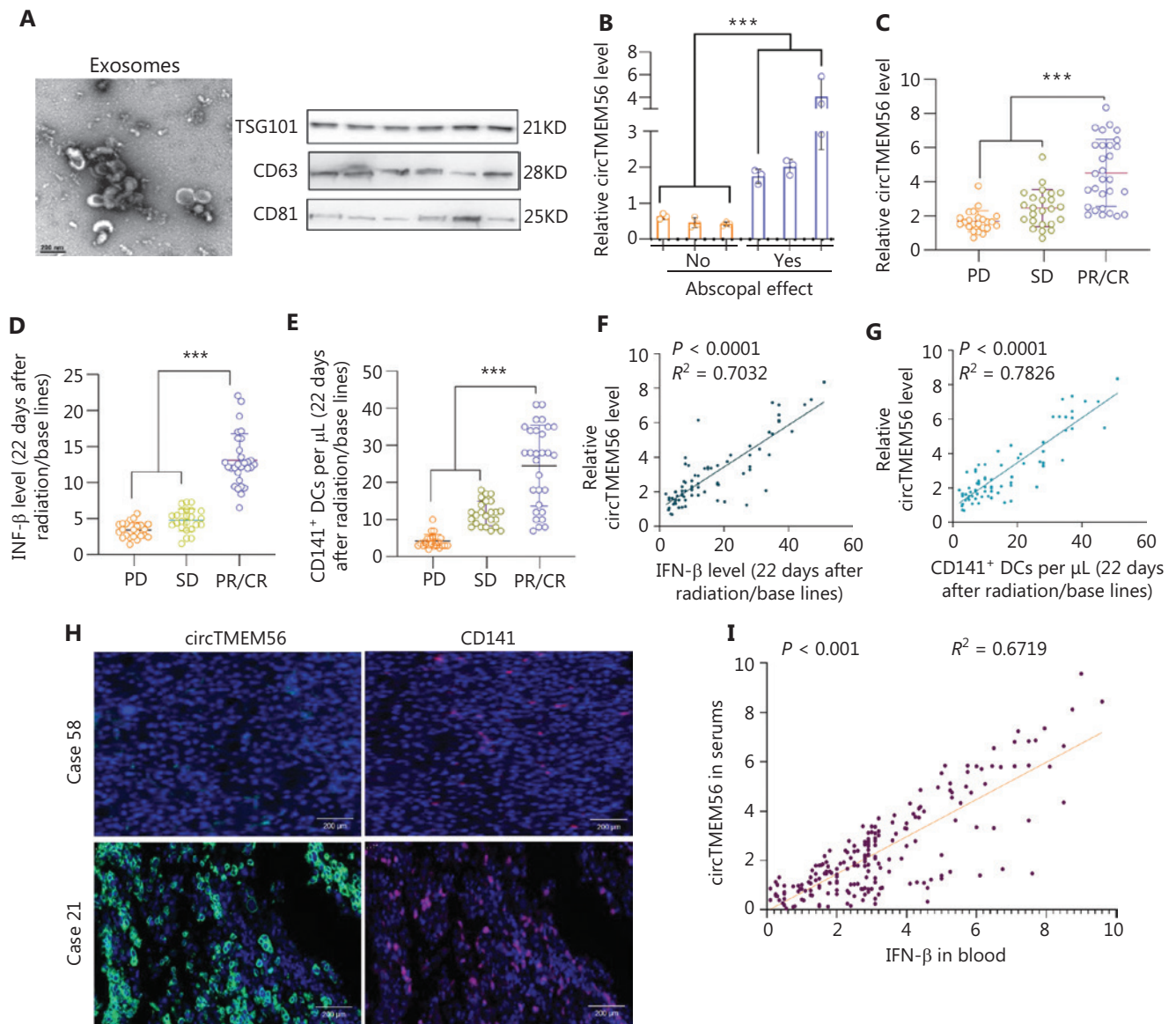


**Figure 2** Exosome circTMEM56 from hepatocellular carcinoma (HCC) cells is associated with the radiotherapy (RT) effect. (A) Representative image of exosomes extracted from patient blood using ultracentrifugation. Exosome markers are detected on exosomes enriched in patient blood. (B) circTMEM56 expression in patient blood with an abscopal effect (AE) is significantly higher than patients without AEs. (C) circTMEM56 levels in the blood of 76 patients with HCC after RT analyzed by qPCR. (D) Interferon-beta (IFN- $\beta$ ) levels in the blood of 76 patients with HCC after RT analyzed by ELISA. (E) Number of cDC1s in the blood of 76 patients with HCC after RT. (F) Correlation analysis showing a positive relationship between circTMEM56 and the IFN- $\beta$  level. (G) Correlation analysis showing a positive relationship between circTMEM56 and the number of cDC1s. (H) Representative images of circTMEM56 and CD141 staining in HCC. (I) Correlation analysis showing a positive relationship between circTMEM56 and the IFN- $\beta$  level in 209 patients with HCC. \*\*\* $P < 0.001$ .

biotinylated miR-136-5p mimics significantly enriched circTMEM56 during pulldown assays compared to negative controls (**Figure 4D**). Moreover, fluorescence in situ hybridization (FISH) analyses of cancer cells demonstrated that circTMEM56 co-localizes with miR-136-5p (**Figure 4E**). The impact of circTMEM56 overexpression on the proteome was

determined using liquid chromatography-tandem mass spectrometry (LC-MS/MS)-based quantitative proteomic analysis with SILAC to confirm the miR-136-5p targets. Nearly 7,000 annotated proteins were identified in DC-circTMEM56 and -control cells. Among these 7,000 proteins, 435 and 501 were up- and down-regulated, respectively, in the

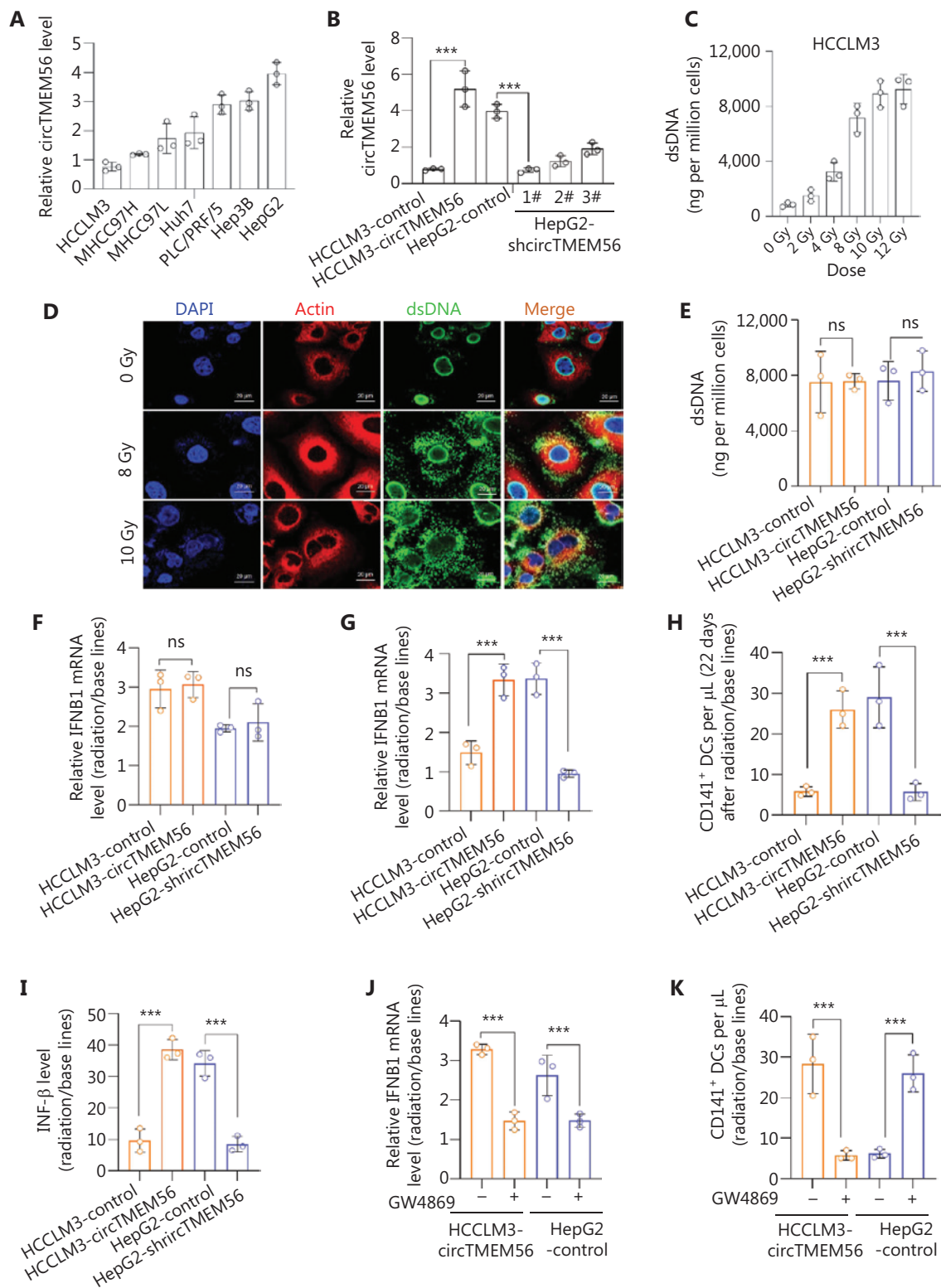


**Figure 3** circTMEM56 increases the production of type I IFN (IFN-I) from dendritic cells (DCs) and mediates an anti-tumor immune response. (A) circTMEM56 level measured by qPCR in 7 different hepatocellular carcinoma (HCC) cell lines. (B) Efficacy of circTMEM56 overexpression and interference analyzed by qRT-PCR. (C) dsDNA content in the cell supernatant following different radiation doses. (D) Extracellular dsDNA content detected by immunofluorescence after different radiation doses. (E) Effects of circTMEM56 overexpression and knockdown on dsDNA



release from hepatocellular carcinoma cells after radiation. (F) Effects of circTMEM56 overexpression and knockdown on IFNB1 mRNA levels in hepatocellular carcinoma cells after radiation. (G) IFNB1 mRNA levels in DCs after co-culturing with irradiated liver cancer cells. (H) Number of DCs after co-culturing with irradiated liver cancer cells. (I) IFN- $\beta$  concentration in the supernatant after co-culturing of DCs with irradiated hepatocellular carcinoma cells. (J) Changes in IFNB1 mRNA levels in DCs after co-culturing with irradiated HCCs with or without GW4869. (K) Number of DCs after co-culturing with irradiated hepatocellular carcinoma cells with or without GW4869. \*\*\* $P < 0.001$ .

DC-circTMEM56 cells (**Figure 4F**). Functional analysis using GO and KEGG indicated that the differentially expressed proteins in DC-circTMEM56 cells were primarily associated with the immune response, chemotaxis, the inflammatory response, cell adhesion, angiogenesis, positive regulation of cell migration, and the PI3K-Akt, the TNF, and chemokine signaling pathways (**Figure 4G**). Western blot analysis confirmed that circTMEM56 expression increases the STING protein and related cytokines levels, which was consistent with the quantitative proteomic analysis (**Figure 4H**). Independent transcriptomic and proteomic analyses revealed that circTMEM56 affects the cGAS-STING pathway in DCs.

STING may be a human target of miR-136-5p based on RNA-seq results and online prediction (**Figure 4I**). Initially, the potential binding sites between STING and miR-136-5p were identified. Subsequent dual-luciferase reporter assays demonstrated a decrease in luciferase activity in cells transfected with WT miR-136-5p compared to cells transfected with mutant miR-136-5p (**Figure 4J**). To better understand miR-136-5p functions in circTMEM56-induced signaling, lentiviral vectors expressing miR-136-5p and miR-136-5p inhibitors were constructed and stable DCs were established. STING and IFN- $\beta$  expression were upregulated in DC-shmiR-136-5p and DC-circTMEM56 (**Figure 4K, L**). Additionally, corresponding changes in IFN- $\beta$  expression were noted (**Figure 4M**). Given that circTMEM56 overexpression compromised the immune microenvironment in DCs *via* the miR-136-5p/STING1 axis, we concluded that circTMEM56 overexpression promotes HCC progression.

### Elevated exosome circTMEM56 specifically targets DCs to facilitate the cGAS-STING pathway in HCC

The innate immune sensor, cGAS-STING, has a critical role in tumors and immune cells and can be activated in tumor cells, DCs, and macrophages to regulate various stages of the cancer-immunity cycle. The role of these cells in RT-induced anti-tumor immune responses in HCC was investigated.

Measurement of miR-136-5p levels in THP-1 cells, macrophages, and DCs showed that DCs expressed higher miR-136-5p levels compared to THP-1 cells and macrophages (**Figure 5A**). Furthermore, HCCLM3-circTMEM56 and HepG2-shcircTMEM56 cells modulated STING expression in DCs, but not THP-1 cells or macrophages (**Figure 5B**). When co-cultured with CD8<sup>+</sup> T cells, IFN- $\beta$  expression in THP-1 and M2 macrophages remained unchanged under HCCLM3-circTMEM56 and HepG2-shcircTMEM56 cell treatment (**Figure 5C, D**), indicating that circTMEM56 influenced the expression of STING in DCs. The cGAS-STING pathway reached maximum activation in DCs expressing circTMEM56 at 72 h, as demonstrated by the dose-response experiments (**Figure 5E**). By measuring the effect of circTMEM56 on the cGAS-STING pathway in DCs, p-STING and p-IRF3 levels were shown to be higher after treatment with the supernatant from HCCLM3-circTMEM56 cells following RT compared to the supernatant from HCCLM3-control cells after RT. The increase in miR-136-5p expression was suppressed or counteracted by STING overexpression (**Figure 5F–H**), as confirmed by multiplex immunofluorescence (mIF) in HCC tissues post-RT (**Figure 5I**). These data indicated that circTMEM56 overexpression specifically influences the cGAS-STING pathway.

### Exosome circTMEM56 improves RT-induced anti-tumor immunity in HCC

Based on these findings it was predicted that circTMEM56 could improve the tumor response to RT in mice with HCC. Hepa1-6-circTMEM56 and Hepa1-6-control *in situ* tumor models were constructed in TMEM173 and cGASWT, as well as TMEM173KO and cGASKO mice, and subsequently treated with RT (8 GyX3). Tumor growth was significantly delayed in Hepa1-6-circTMEM56 tumors compared to Hepa1-6-control tumors in TMEM173 and cGASWT mice. However, Hepa1-6-circTMEM56 *in situ* tumors exhibited growth rates like Hep1-6-control *in situ* tumors in TMEM173 and cGASWT mice but unlike the delayed growth observed in TMEM173KO and

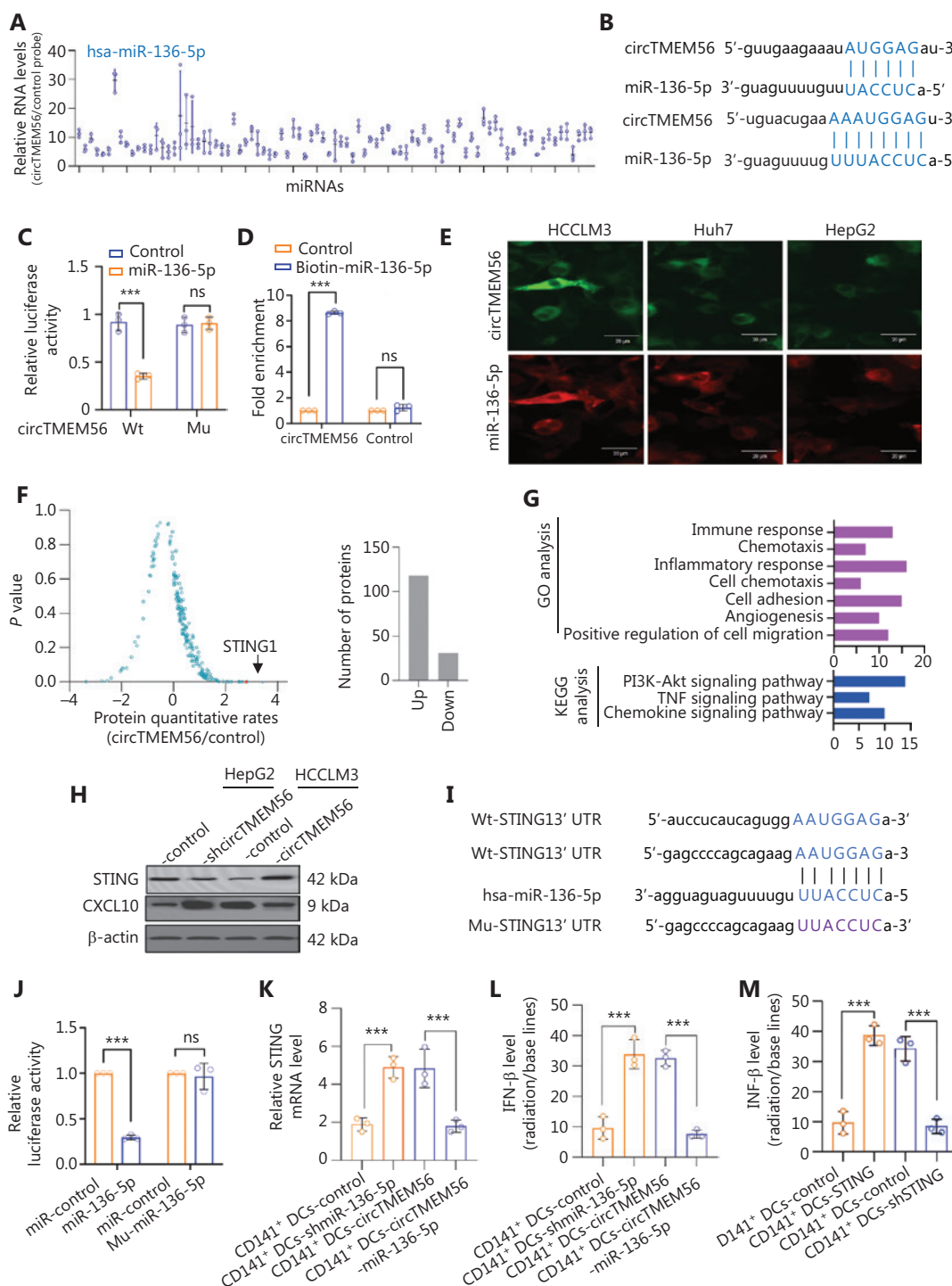


**Figure 4** circTMEM56 amplifies radiotherapy (RT)-induced anti-tumor immune response through the miR-136-5p/STING1 axis in dendritic cells (DCs). (A) RIP was performed for circRNA in DCs using a circTMEM56 probe and a negative control (NC) probe. (B) Putative binding sites of miR-136-5p with respect to circTMEM56 predicated *via* StarBase v3.0. (C) Luciferase activity of pLG3-circTMEM56 in 293T cells after co-transfection with miR-136-5p. (D) circTMEM56 levels in the streptavidin-captured fractions of the 293T cell lysates after transfection with biotinylated miR-136-5p or the NC. (E) FISH analysis in hepatocellular carcinoma (HCC) showing co-localization of circTMEM56 with miR-136-5p in the cytoplasm. (F) A graph showing overlap of differentiated proteins. (G) GO and KEGG analyses were performed. (H) Levels of STING and CXCL10 protein expression in DCs with varying levels of circTMEM56 expression detected by western blot analysis. (I) Putative

binding site of miR-136-5p on STING via StarBase v3.0. (J) Luciferase activity of pLG3-STING in 293T cells co-transfected with miR-136-5p. (K) STING mRNA levels in DCs expressed by different miR-136-5p or circTMEM56. (L) Interferon- $\beta$  (IFN- $\beta$ ) levels in DC supernatant detected after co-culturing with irradiated HCC cells with different levels of miR-136-5p or circTMEM56 expression. (M) IFN- $\beta$  levels in DCs supernatant after co-culturing with irradiated HCC cells and varying levels of STING expression. \*\*\* $P < 0.001$ .

cGASKO mice (**Figure 6A, B**). The administration of exosome circTMEM56 delayed the growth of *in situ* Hepa1-6-control tumors in Teme173 and cGASWT mice but this effect was not noted in STING-deficient (TMEM173KO) and cGASKO mice (Mb21d1-/-). Importantly, a significant increase in the number of DCs and CD8<sup>+</sup> T cells was observed in Hepa1-6-circTMEM56 tumors and Hepa1-6-control tissues treated with exosome circTMEM56 derived from Teme173 and cGASWT mice following RT compared to the corresponding control groups (**Figure 6C, D**).

A subcutaneous tumor model was established by injecting Hepa1-6-circTMEM56 and Hepa1-6-control every 2 d, followed by RT on the previously injected tumor. When comparing Hepa1-6-circTMEM56 with Hep1-6-control, non-irradiated tumor lesions steadily regressed in the groups treated with exosome circTMEM56 (**Figure 6E**). In conclusion, circTMEM56 enhanced anti-tumor immunity in DCs by activating the cGAS-STING pathway.

## Discussion

Although the role of RT in modulating the tumor microenvironment has been recognized for years, our understanding of the molecular mechanisms by which RT influences innate and adaptive immune responses continues to evolve. The current study revealed that patients with HCC who exhibited AEs after RT had elevated circTMEM56 levels in tissues and serum compared to RT-resistant patients. We suggest that low circTMEM56 levels are associated with longer overall survival and lower recurrence rates in patients with HCC. The results of the current study revealed that elevated circTMEM56 expression enhances cGAS-STING signaling through the miR-136-5p/STING axis during tumor cell-to-DC communication (**Figure 7**). According to the findings herein, elevated circTMEM56 augmented the number of tumor-infiltrating CD8<sup>+</sup> T cells and serum IFN- $\beta$  level in transgenic mice with HCC. Administering exosome circTMEM56 significantly improved the response to RT in tumors with low circTMEM56 levels, highlighting the clinical importance. These

findings suggest that using exosome circTMEM56 could serve as a novel adjuvant to conventional RT by resetting the tumor immunomicroenvironment.

The cGAS-STING pathway has an important role in regulating immune responses<sup>17</sup>. Through cGAS-STING-IFN-mediated immune activation, RT stimulates anti-tumor immunity<sup>18-20</sup>. The tumor microenvironment exhibits highly complex cGAS-STING signaling activation and influences different cell types, such as cancer cells, DCs, and macrophages. Activating the cGAS-STING pathway in tumor cells can act as a barrier to the early progression of cancer by promoting IFN-I expression and other pro-inflammatory genes. Furthermore, this pathway is strongly associated with triggering cellular senescence in cancer cells, which contributes to tumor-suppressive effects<sup>21</sup>. The findings herein revealed that exosome circTMEM56 selectively increased STING expression in DCs without affecting HCC and macrophages, which was attributed to low STING levels in HCC and reduced miR-136-3p in macrophages. Based on the observation that cGAS-STING activation facilitates tumor progression in mice<sup>22-24</sup> and drives liver inflammation in macrophages, the effects of exosome circTMEM56 on HCC xenografts were confirmed in several mouse models, including transgenic models. The findings herein provide novel evidence for the role of cGAS-STING signaling in RT-induced immune responses and suggest a therapeutic strategy for enhancing anti-tumor immunity. However, further investigation is needed to identify the precise mechanisms by which the cGAS-STING pathway enhances RT efficacy in tumor cells.

Intercellular communication relies heavily on exosomes, which act as messengers carrying bioactive molecules<sup>25</sup>. The recent discovery of circRNAs in exosomes has attracted significant attention due to the enrichment and stability. Aberrant circRNA expression has been implicated in various diseases, particularly cancer. For example, exosome circUHRF1 induces NK cell dysfunction and contributes to immunosuppression and resistance to anti-PD-1 immunotherapy in HCC. Additionally, through the miR-934/SHP2 axis, the

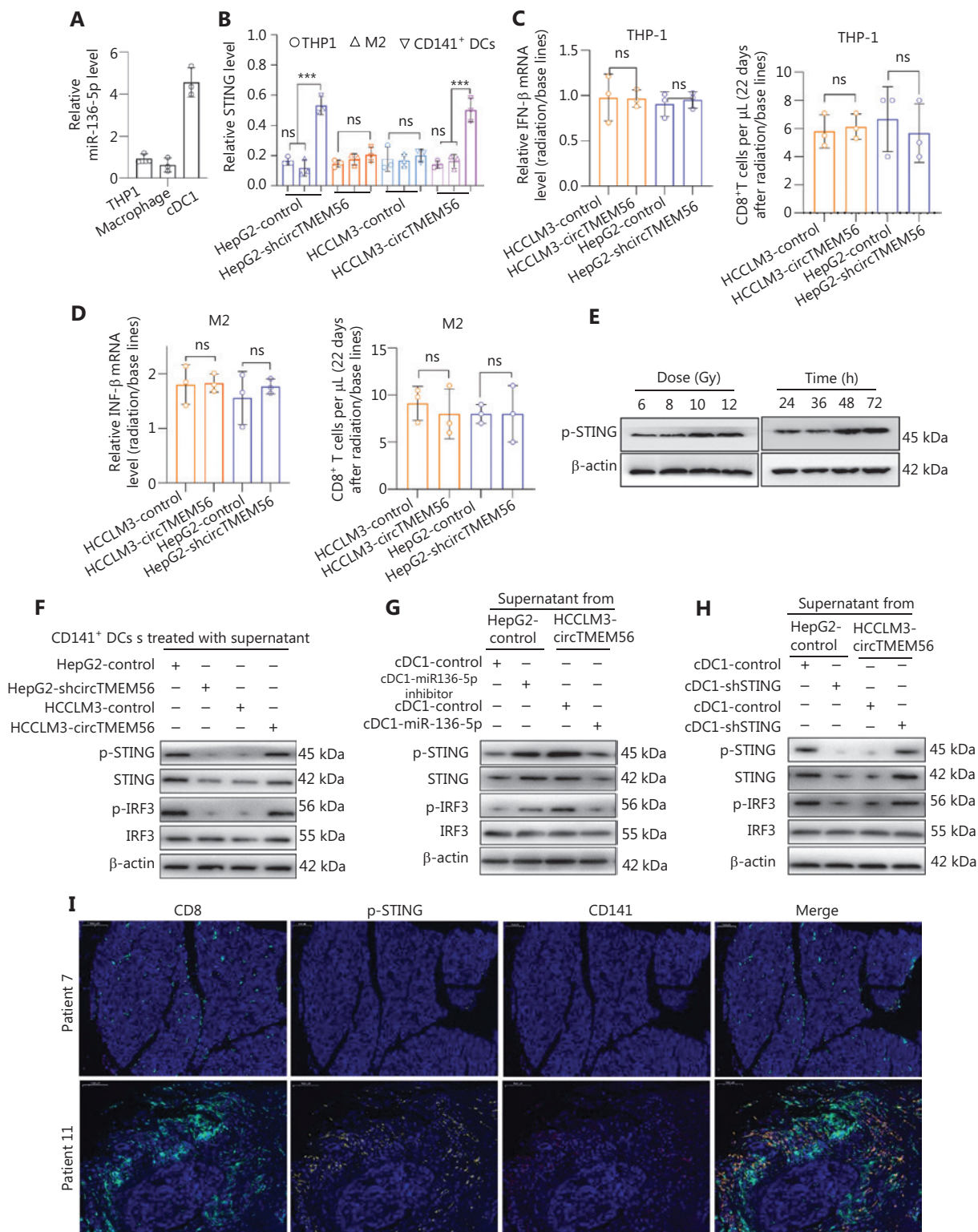


**Figure 5** Elevated exosome circTMEM56 specifically targets dendritic cells (DCs) and promotes activation of cGAS-STING pathway. (A) Relative levels of miR-136-5p in THP-1, macrophages, and cDC1 detected by qPCR. (B) Levels of STING expression in THP-1, M2 macrophages, and cDC1 cultured in conditioned medium and detected by qPCR. (C) Interferon-β (IFN-β) levels in the supernatant of THP-1 cells after co-culturing with irradiated liver cancer cells and the number of CD8<sup>+</sup> T cells detected after co-culturing with CD8<sup>+</sup> T cells. (D) IFN-β levels



in the supernatant of M2 macrophages after co-culturing with irradiated liver cancer cells and the number of CD8<sup>+</sup> T cells detected after co-culturing with CD8<sup>+</sup> T cells. (E) Activation of STING detected by western blot at different radiation doses and time points. (F) Western blot analysis of STING pathway activation in DCs cultured in different conditioned media. (G) Western blot analysis of STING pathway activation in DCs cultured with different miR-136-5p levels in different conditioned media. (H) Western blot analysis to detect STING pathway activation in DCs with different levels of STING expression cultured in different conditioned media. (I) Representative images of CD8, CD141, and p-STING staining in HCC tissues. \*\*\* $P < 0.001$ .

exosome circuit reshapes the tumor microenvironment in non-small cell lung cancer by promoting CD8<sup>+</sup> T-cell dysfunction. The development of novel therapeutic and diagnostic strategies utilizing exosomes for cancer treatment has been facilitated by studies on exosome characteristics during tumor pathogenesis. Bioengineered exosomes, which create an optimal microenvironment for immunomodulatory factors, have shown great potential as cancer immunotherapies. Bioengineered exosomes effectively activate stages of the cancer immunity cycle to induce strong cancer-specific immune responses. By co-culturing DCs with circTMEM56, higher levels of exosome circTMEM56 were shown to significantly augment DC proliferation and activation, enhancing IFN-1 $\beta$  production. Notably, the administration of exosome circTMEM56 improved RT efficacy by boosting anti-tumor immunity. The results of the current study suggested that exosome circTMEM56 may be an effective adjuvant for RT in patients with HCC. The delivery of circTMEM56 *via* exosomes represents an advanced research domain that capitalizes on the biocompatibility, stability, and targeting capabilities of exosomes. Techniques, such as parental cell transfection, direct loading, or electroporation, could be used to incorporate circTMEM56 into exosomes. Nevertheless, some persistent challenges include exosome purification, maintenance of circTMEM56 stability and activity, and evaluation of circTMEM56 safety and efficacy. With advances in technology, more efficient and secure delivery methodologies are anticipated to emerge, thereby facilitating the clinical application of circTMEM56.

In addition to identifying the molecular mechanism by which circTMEM56 enhances the radiotherapy-induced tumor immunomicroenvironment, the current study offers a novel and effective adjuvant for HCC radiotherapy in a specific subgroup of patients. A theoretical basis is provided for developing combination therapies to further improve the survival rate of patients with HCC and reduce recurrences. A preliminary clinical trial involving 34 patients with advanced HCC was conducted to determine the role of circTMEM56 in RT combined with anti-PD-1 therapy. The results indicated

that higher levels of circTMEM56 expression were significantly associated with increased response rates and improved overall survival, suggesting that circTMEM56 may serve as a potential biomarker for predicting therapeutic outcomes in HCC patients. However, given the limited sample size, these findings warrant further validation through large scale corollary studies (Figure S1).

## Conclusions

The findings of the current study showed that circTMEM56 enhances RT efficacy in HCC by serving as a competitive endogenous RNA to sponge miR-136-5p, thereby alleviating suppression of STING and activating the cGAS-STING signaling pathway. Elevated circTMEM56 levels correlated with increased tumor-infiltrating CD8<sup>+</sup> T cells, elevated serum IFN- $\beta$  levels, and improved clinical outcomes in HCC patients. Exosome circTMEM56 specifically targets DCs to amplify cGAS-STING-driven anti-tumor immunity, highlighting the potential of exosome circTMEM56 as a therapeutic adjuvant to augment the RT response. These findings underscore the role of circTMEM56 in reshaping the immunomicroenvironment and propose a novel strategy for optimizing RT efficacy in HCC. Further validation through large-scale clinical trials is essential to translate these insights into actionable therapeutic interventions.

## Grant support

This study was funded by the National Key Research and Development Program of China (Grant No. 2023YFC3402700), Shanghai Municipal Natural Science Foundation (Grant No. 22ZR1411200), China Postdoctoral Science Fund-General Fund (Grant No. 2022M720779), Research Fund of Zhongshan Hospital Affiliated to Shanghai Fudan University for Young Scientists (Grant No. 2023ZSQN26), and National Natural Science Foundation of China (Grant Nos. 82403999 and 82073479).

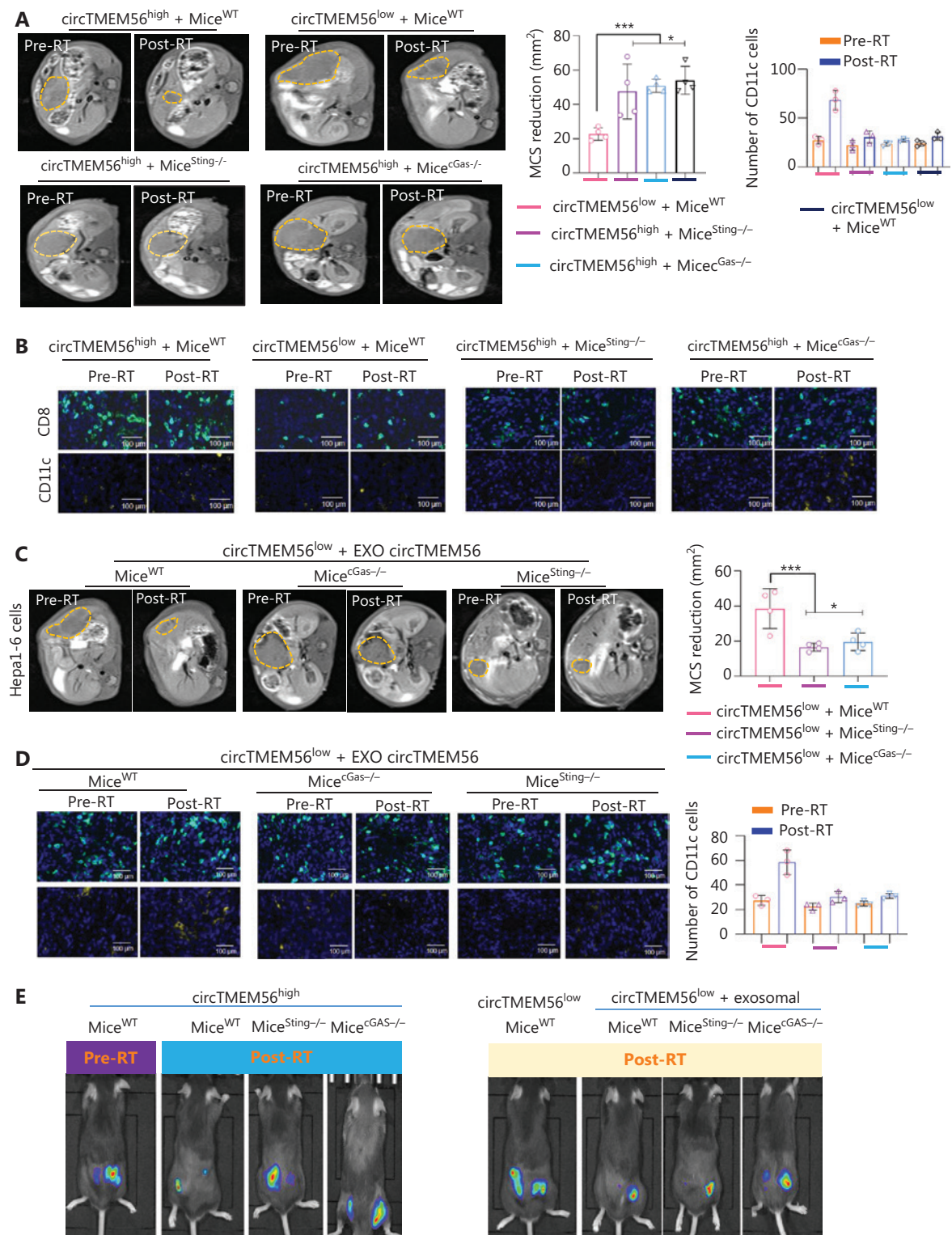


**Figure 6** Exosome circTMEM56 improves the radiotherapy (RT)-induced anti-tumor immunity efficacy *in vivo*. (A) Representative CT images of the abdomen of mice with corresponding quantification. (B) Representative images of CD8 and CD11c staining in hepatocellular carcinoma (HCC). (C) Representative CT images of the abdomen of mice with corresponding quantification. (D) Representative images of CD8 and CD11c staining in HCC. (E) Representative photographs of the Hepa1-6 subcutaneous tumor model, imaged using the IVIS Imaging System. \* $P < 0.05$ ; \*\*\* $P < 0.001$ .

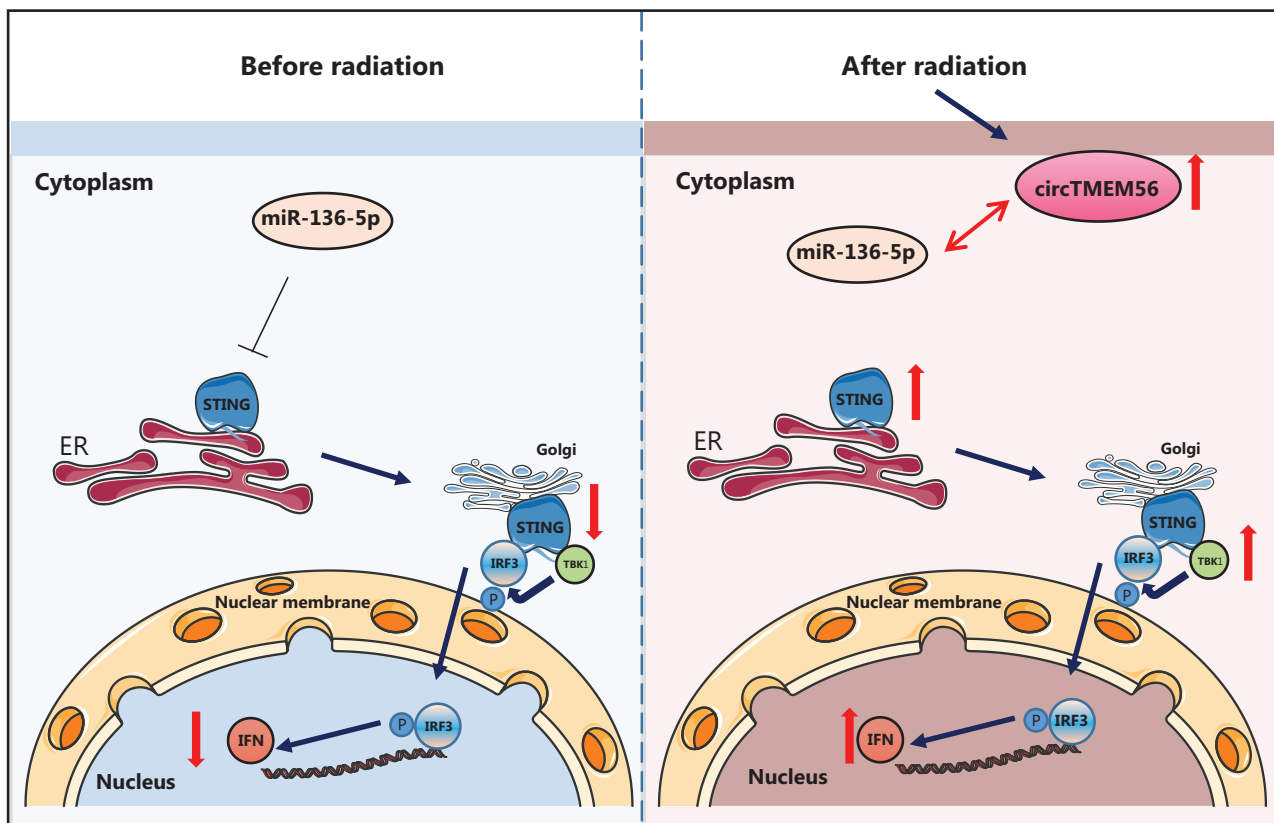


**Figure 7** Working model: circTMEM56 regulates cGAS-STING signaling pathway in DCs. miR-136-5p in the cytoplasm exerts an inhibitory effect on the STING activation before radiation (left panel). Under normal conditions STING is activated when DCs detect dsDNA released by tumor cells. Once activated STING moves from the endoplasmic reticulum to the Golgi apparatus, where STING interacts with TBK1 on the Golgi membrane. However, the inhibitory action of miR-136-5p impairs STING activity and prevents STING translocation and interaction with TBK1, thereby disrupting IRF3 phosphorylation and leading to suppression of downstream IFN signaling. Consequently, the STING signaling pathway remains in a relatively inactive state, limiting immune activation and impairing IFN-mediated responses. Radiation induces the upregulation of circTMEM56 in the cytoplasm (right panel), which acts as a ceRNA to sponge miR-136-5p, thereby reducing the inhibitory effects on STING signaling. Consequently, activation of STING leads to enhanced recruitment of TBK1 and phosphorylation of IRF3. Phosphorylated IRF3 translocates into the nucleus, where phosphorylated IRF3 binds to specific promoter regions of DNA and promotes the expression of IFN. This radiation-induced enhancement of STING activation suggests a potential mechanism for improving anti-tumor immunity through regulation of circRNA-miRNA interactions. circTMEM56, circular RNA TMEM56; ER, endoplasmic reticulum; IFN, interferon; IRF3, interferon regulatory factor 3; miR-136-5p, microRNA-136-5p; STING, Stimulator of Interferon Genes; TBK1, TANK-binding kinase 1.

## Conflict of interest statement

No potential conflicts of interest are disclosed.

## Author contributions

Conceived and designed the analysis: Shisuo Du, Keai wu, Chao Gao.

Collected the data: Junjie Cheng, Shilin Lin, Aying Ma, Zhaochong Zeng.

Contributed data or analysis tools: Li Yuan, Kunchao Li, Yiming Zheng.

Performed the analysis: Li Yuan, Yue Wang, Junjie Cheng.

Wrote the paper: Li Yuan, Chao Gao, Yue Wang.

## Data availability statement

The datasets used and/or analyzed in the current study are available from the corresponding author upon reasonable request.

## References

- Bray F, Laversanne M, Sung H, Ferlay J, Siegel RL, Soerjomataram I, et al. Global cancer statistics 2022: GLOBOCAN estimates of incidence and mortality worldwide for 36 cancers in 185 countries. *CA Cancer J Clin.* 2024; 74: 229-63.
- Dimitroulis D, Damaskos C, Valsami S, Davakis S, Garmpis N, Spartalis E, et al. From diagnosis to treatment of hepatocellular carcinoma: an epidemic problem for both developed and developing world. *World J Gastroenterol.* 2017; 23: 5282-94.
- Mondini M, Levy A, Meziani L, Milliat F, Deutsch E. Radiotherapy-immunotherapy combinations – perspectives and challenges. *Mol Oncol.* 2020; 14: 1529-37.
- Chen LL. The biogenesis and emerging roles of circular RNAs. *Nat Rev Mol Cell Biol.* 2016; 17: 205-11.
- Patop IL, Kadener S. circRNAs in Cancer. *Curr Opin Genet Dev.* 2018; 48: 121-7.
- Zhang PF, Wei CY, Huang XY, Peng R, Yang X, Lu JC, et al. Circular RNA circTRIM33-12 acts as the sponge of MicroRNA-191 to suppress hepatocellular carcinoma progression. *Mol Cancer.* 2019; 18: 105.
- Zhang PF, Gao C, Huang XY, Lu JC, Guo XJ, Shi GM, et al. Cancer cell-derived exosomal circUHRF1 induces natural killer cell exhaustion and may cause resistance to anti-PD1 therapy in hepatocellular carcinoma. *Mol Cancer.* 2020; 19: 110.
- Schreiber RD, Old LJ, Smyth MJ. Cancer immunoediting: integrating immunity's roles in cancer suppression and promotion. *Science.* 2011; 331: 1565-70.
- Dunn GP, Bruce AT, Ikeda H, Old LJ, Schreiber RD. Cancer immunoediting: from immunosurveillance to tumor escape. *Nat Immunol.* 2002; 3: 991-8.
- Allison JP. Immune checkpoint blockade in cancer therapy: the 2015 Lasker-DeBakey clinical medical research award. *JAMA.* 2015; 314: 1113-4.
- El-Khoueiry AB, Sangro B, Yau T, Crocenzi TS, Kudo M, Hsu C, et al. Nivolumab in patients with advanced hepatocellular carcinoma (CheckMate 040): an open-label, non-comparative, phase 1/2 dose escalation and expansion trial. *Lancet.* 2017; 389: 2492-502.
- Zhu AX, Finn RS, Edeline J, Cattan S, Ogasawara S, Palmer D, et al. Pembrolizumab in patients with advanced hepatocellular carcinoma previously treated with sorafenib (KEYNOTE-224): a non-randomised, open-label phase 2 trial. *Lancet Oncol.* 2018; 19: 940-52.
- Wei CY, Zhu MX, Zhang PF, Huang XY, Wan JK, Yao XZ, et al. PKC $\alpha$ /ZFP64/CSF1 axis resets the tumor microenvironment and fuels anti-PD1 resistance in hepatocellular carcinoma. *J Hepatol.* 2022; 77: 163-76.
- de Mingo Pulido Á, Gardner A, Hiebler S, Soliman H, Rugo HS, Krummel MF, et al. TIM-3 regulates CD103<sup>+</sup> dendritic cell function and response to chemotherapy in breast cancer. *Cancer Cell.* 2018; 33: 60-74.e6.
- Xie N, Cai JB, Zhang L, Zhang PF, Shen YH, Yang X, et al. Upregulation of B7-H4 promotes tumor progression of intrahepatic cholangiocarcinoma. *Cell Death Dis.* 2017; 8: 3205.
- Hansen TB, Jensen TI, Clausen BH, Bramsen JB, Finsen B, Damgaard CK, et al. Natural RNA circles function as efficient microRNA sponges. *Nature.* 2013; 495: 384-8.
- Li T, Chen ZJ. The cGAS-cGAMP-STING pathway connects DNA damage to inflammation, senescence, and cancer. *J Exp Med.* 2018; 215: 1287-99.
- Twyman-Saint Victor C, Rech AJ, Maity A, Rengan R, Pauken KE, Stelekati E, et al. Radiation and dual checkpoint blockade activate non-redundant immune mechanisms in cancer. *Nature.* 2015; 520: 373-7.
- Rudqvist NP, Pilonis KA, Lhuillier C, Wennerberg E, Sidhom JW, Emerson RO, et al. Radiotherapy and CTLA-4 blockade shape the TCR repertoire of tumor-infiltrating T cells. *Cancer Immunol Res.* 2018; 6: 139-50.
- Dovedi SJ, Cheadle EJ, Popple AL, Poon E, Morrow M, Stewart R, et al. Fractionated radiation therapy stimulates antitumor immunity mediated by both resident and infiltrating polyclonal T-cell populations when combined with PD-1 blockade. *Clin Cancer Res.* 2017; 23: 5514-26.
- Jiang M, Chen P, Wang L, Li W, Chen B, Liu Y, et al. cGAS-STING, an important pathway in cancer immunotherapy. *J Hematol Oncol.* 2020; 13: 81.
- Bakhoum SF, Ngo B, Laughney AM, Cavallo JA, Murphy CJ, Ly P, et al. Chromosomal instability drives metastasis through a cytosolic DNA response. *Nature.* 2018; 553: 467-72.
- Bakhoum SF, Landau DA. Chromosomal instability as a driver of tumor heterogeneity and evolution. *Cold Spring Harb Perspect Med.* 2017; 7: a029611.
- Dou Z, Ghosh K, Vizioli MG, Zhu J, Sen P, Wangenstein KJ, et al. Cytoplasmic chromatin triggers inflammation in senescence and cancer. *Nature.* 2017; 550: 402-6.
- Xu M, Ji J, Jin D, Wu Y, Wu T, Lin R, et al. The biogenesis and secretion of exosomes and multivesicular bodies (MVBs): intercellular shuttles and implications in human diseases. *Genes Dis.* 2022; 10: 1894-907.

**Cite this article as:** Yuan L, Wang Y, Cheng J, Lin S, Ma A, Li K, et al. Cancer-derived exosomal circTMEM56 enhances the efficacy of HCC radiotherapy through the miR-136-5p/STING axis. *Cancer Biol Med.* 2025; 22: 396-411. doi: 10.20892/j.issn.2095-3941.2024.0544